Available online at www.sciencedirect.com
SCIENCE DIRECT®
Journal of Molecular Catalysis A: Chemical 225 (2005) 143–148
JOURNAL OF MOLECULAR CATALYSIS A: CHEMICAL
www.elsevier.com/locate/molcata

Comparison of bulk CoMo bimetallic carbide, oxide, nitride and sulfide catalysts for pyridine hydrodenitrogenation

Hamid A. Al-Megren[a,b], Tiancun Xiao[a,*], Sergio L. Gonzalez-Cortes[a], Soliman H. Al-Khowaiter[b], Malcolm L.H. Green[a]

[a] *The Wolfson Catalysis Center, Inorganic Chemistry Laboratory, University of Oxford, South Parks Road, OX1 3QR, UK.*
[b] *Petroleum and Petrochemicals Research Institute, King Abdulaziz City for Science and Technology, P. O. Box 6086, Riyadh 11442, Saudi Arabia*

Received 14 June 2004; accepted 31 August 2004
Available online 8 October 2004

Abstract

Bimetallic cobalt–molybdenum oxide ($CoMoO_x$) has been prepared and converted into $CoMoN_x$, $CoMoC_x$ and $CoMoS_x$ materials by temperature-programmed reactions with ammonia, ethane or hydrogen sulfide, respectively. These new bimetallic materials have been characterised using X-ray diffraction (XRD) and solid state NMR and tested for pyridine hydrodenitrogenation (HDN) at various temperatures. The initial HDN activity of the catalysts decreases in order $CoMoC_x \sim CoMoN_x \sim CoMoO_x > CoMoS_x$. The stability order of the first three of catalysts is $CoMoC_x > CoMoN_x > CoMoO_x$, and their activities decrease with the time on stream. In contrast the pyridine conversion over $CoMoS_x$ is more stable and activity increases with the time on stream, from 30 to over 50%, this is accompanied by the formation of $CoMoSC_x$ material. The high catalytic activity of the $CoMoC_x$ catalyst may reflect the ability to hydrocrack pyridine to yield methane. The $CoMoS_x$ catalyst system has the highest selectivity to the products cyclopentane (35%) and pentane (27%).

Keywords: CoMo catalyst; Carbide; Nitride; Sulfide; Pyridine HDN

1. Introduction

Over the past two decades the average quality of petroleum has diminished by approximately two points on the American Petroleum Institute (API) gravity scale [1], implying the increase of the density of petroleum and rise of heteroatom content. These changes require the use of more robust catalysts to remove the heteroatom content to meet the increasingly the stringent regulations. The hydrodenitrogenation (HDN) process to remove nitrogen heteroatom from crude oil is a hydrotreating processes. Typical industrial catalysts used contain Co–Mo sulfides or Ni–Mo sulfides supported on alumina. However, these catalysts are not efficient enough and recent research has sought to develop more effective HDN catalysts.

Transition metal-carbides and -nitrides have shown excellent HDN activity, with high selectivities for the formation of aromatic products. [2–10] Schlatter et al. [2] found that molybdenum nitride and molybdenum carbide catalysts were more active than a commercial $Ni–Mo/Al_2O_3$ sulfide catalyst, and they required less hydrogen for the HDN of quinoline. Oyama showed that HDN activity for quinoline activity using early transition metal carbides followed the order, group 6 > group 5 > group 4 [6]. Supported and unsupported bimetallic Nb–Mo carbides showed enhanced activity and stability compared to the corresponding monometallic carbides. [9,10] However, there are no reports of the comparison of bimetallic CoMo carbide, nitride and sulfide catalysts for HDN performance. In our previous studies, we have found that the $Co_4Mo_6C_x$ has the highest performance for pyridine

* Corresponding author. Tel.: +44 1865 272660; fax: +44 186 5272690.
E-mail address: xiao.tiancun@chem.ox.ac.uk (T. Xiao).

1381-1169/$ – see front matter © 2004 Elsevier B.V. All rights reserved.
doi:10.1016/j.molcata.2004.08.041

HDN [11–13]. Hence it was decided to make a systematic study to compare the performance of the bimetallic CoMo nitride, carbide and sulfide catalysts for HDN, as described below.

2. Experimental

The CoMo oxide, carbide, nitride and sulfide samples were prepared with the same Co/Mo ratio of 0.67. The oxide $Co_4Mo_6O_x$ was prepared as reported previously [11]. For the preparation of the bimetallic carbide $Co_4Mo_6C_x$ the oxide $Co_4Mo_6O_x$, loaded into a 4 mm i.d. quartz tube housed in a furnace, was treated with a mixture of ethane (10% by volume) and hydrogen with a total flow rate 100 cm^3/min. The temperature was increased at 1 °C/min to 630 °C and held until no carbon oxides were detected in the exhausted gas (GC–MS). The characterization details of the carbide sample are described elsewhere [11].

The nitride $Co_4Mo_6N_x$ was prepared by passing 60 cm^3/min of NH_3 over $Co_4Mo_6O_x$. The temperature of the furnace was raised at 5 °C/min from room temperature to 120 °C, and held for 30 min. Then the temperature was increased at 1 °C/min to 680 °C, and held at this temperature for 3 h.

The sulfide Co_4Mo_6S was prepared by passing a flow of H_2S (10%) and hydrogen (90%) at a combined flow rate of 200 cm^3/min over $Co_4Mo_6O_x$. The sample was heated at 2.5 °C/min to 400 °C and held for 2 h at this temperature.

The oxide, carbide, nitride and sulfide materials were then tested as catalysts for pyridine hydrodenitrification. For the testing of the carbide, nitride and sulfide catalysts they were prepared in situ continuous flow fixed-bed micro-reactor, as described above, and then cooled to 380 °C and treated with hydrogen which had been saturated with pyridine vapour by passing through liquid pyridine in a saturator at 1 atm and 0 °C to form the reaction mixture. The product gases were analysed using a Hewlett-Packard 5890 II gas chromatograph with FID detector and a 1 m packed column.

For testing of the oxide $Co_4Mo_6O_x$, a (0.2 g) sample was first heated in a flow of H_2 (100 cm^3/min), at 2 °C/min to 450 °C and then cooled to 380 °C for 1 h. Then the hydrogen flow was changed to a flow of hydrogen saturated with pyridine vapour, as described above.

For characterization purpose, samples of the fresh catalyst samples were passivated at room temperature in flowing 1% O_2/He before they were exposed to air.

X-ray studies of the pre- and post-reaction catalysts were made using a Philips PW1710 diffractometer with Cu Kα radiation. The surface areas of the catalysts samples before and after reaction were measured using a Micromeritic ASAP 2000. Solid-state ^{13}C MAS NMR measurements were carried out on a CMX-200 NMR spectrometer at a frequency of 50.31 MHz. The strongly metallic samples were diluted to 40% with sodium chloride and ground finely before packing into the 7 mm zirconia rotor, fitted with boron nitride inserts. The spectra were recorded at room temperature using adamantine ($\delta = 29.5$) as the reference.

3. Result and discussion

3.1. Activity of bimetallic catalysts for the HDN of pyridine

The catalytic activity data are shown in Fig. 1. The $Co_4Mo_6C_x$ had the highest activity for pyridine HDN and the conversion for pyridine HDN was 100% for over 140 h without deactivation. The catalyst $Co_4Mo_6N_x$ also showed good stability and gave a high conversion of pyridine for about 50 h. The catalyst activity then decreased slightly, and after 85 h it decreased rapidly. The oxide catalyst $Co_4Mo_6O_x$ showed an initial high HDN activity but this declined rapidly. This behaviour may reflect an initial cracking of the pyridine over cobalt metal particles formed by the pre-treatment of flowing hydrogen, and also with a low surface area of the sample. The HDN of pyridine over $Co_4Mo_6S_x$ increased during the first hours of the reaction and reached the steady state at around 50% after 10 h. The order of the catalyst activity for HDN was $Co_4Mo_6C_x \gg Co_4Mo_6N_x \gg Co_4Mo_6O_x > Co_4Mo_6S_x$.

3.2. Distribution of products of pyridine HDN over different catalysts

Figs. 2–5 shows the distribution of hydrocarbon products with the time on stream for HDN of pyridine over the $Co_4Mo_6O_x$, $Co_4Mo_6N_x$, $Co_4Mo_6C_x$ and $Co_4Mo_6S_x$ catalysts, respectively. Due to the presence of excess of hydrogen gas in the reactants, hydrogenation and hydrogenolysis occur in parallel with thermal cracking. Hence the majority of the products were saturated C_1–C_5 linear hydrocarbons and cyclopentane. Trace amounts of unsaturated hydrocarbons were also detected and were considered together with the corre-

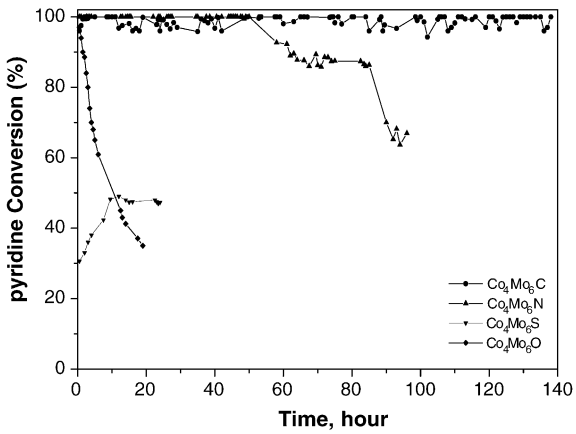

Fig. 1. HDN of pyridine over different phases of CoMo bimetallic catalysts, T: 380 °C, H_2/pyridine ratio: 154, P:1 bar, H_2 flow: 20 ml/min.

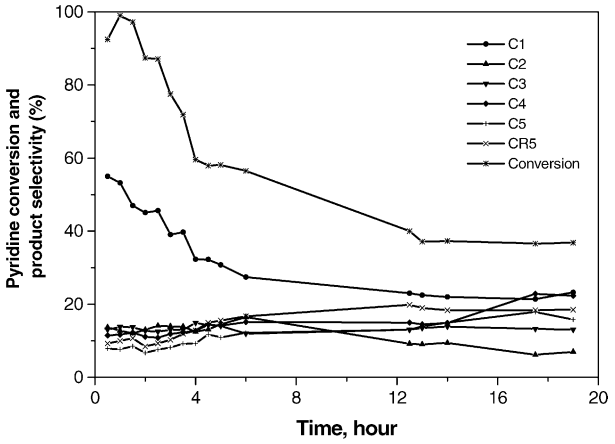

Fig. 2. Changes of product distribution in pyridine HDN over $Co_4Mo_6O_x$ catalyst, T: 380 °C, H_2/pyridine ratio: 154, P:1 bar, H_2 flow: 20 ml/min.

sponding saturated derivatives. The nitrogen was removed as NH_3.

The main reactions occurring in pyridine HDN are hydrogenation, hydrocracking and, in part, hydrogenolysis. At the beginning of the reaction the CoMo oxide, nitride and carbide catalysts show very high hydrocracking activity, producing a large amount of methane. With the time on stream the methane yield decreases, while selectivity to C_5 increases. The product distributions over $Co_4Mo_6C_x$ and $Co_4Mo_6N_x$ suggest that strong hydrogenation and hydrocracking reaction occurred at the beginning of the reaction, leading to the production of smaller hydrocarbons. The high selectivity to CH_4 over $Co_4Mo_6O_x$ may arise from either the hydrocracking of pyridine over the initially formed cobalt metal particle or from the reaction of pyridine with molybdenum oxide material. The decrease in methane selectivity clearly corresponds to the increase of yields of the higher saturated hydrocarbons C_4 and CR_5. The Fig. 3 shows the activity of $Co_4Mo_6N_x$ catalyst decreases after 50 h. The higher HDN activity of the $Co_4Mo_6C_x$ catalyst gives a pyridine conversion of 100% and a lower hydrocarbons in the order $C_1 > C_2 > C_3 > C_4 > C_5 > CR_5$ products (see Fig. 4).

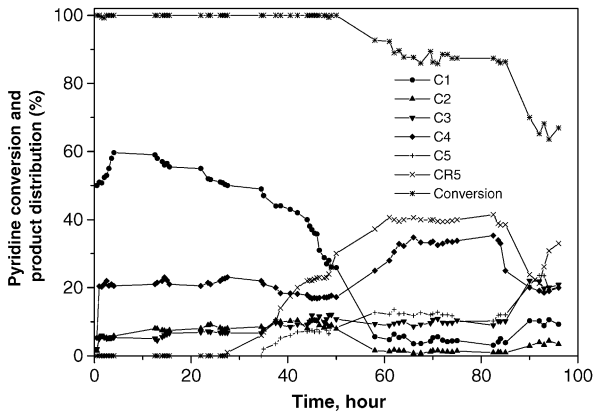

Fig. 3. Changes of product distribution in pyridine HDN over $Co_4Mo_6N_x$ catalyst, T: 380 °C, H_2/pyridine ratio: 154, P:1 bar, H_2 flow: 20 ml/min.

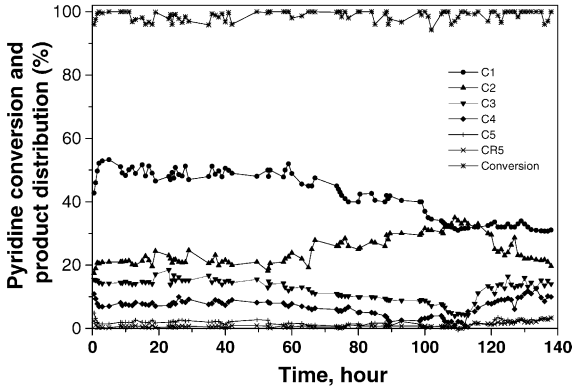

Fig. 4. Changes of product distribution in pyridine HDN over $Co_4Mo_6C_x$ catalyst, T: 380 °C, H_2/pyridine ratio: 154, P:1 bar, H_2 flow: 20 ml/min.

The HDN of pyridine over $Co_4Mo_6S_x$ (see Fig. 5) shows the lowest activity compared to the other catalyst systems. Selectivity to C_5 and CR_5 is higher which suggests that the hydrogenation prevails over hydrocracking.

Due to the high activity and stability of the catalyst $Co_4Mo_6C_x$ [11] it was tested for pyridine HDN over the temperature range 160–400 °C (see Fig. 6). It was found that the conversion of pyridine was lower than 10% between 160–220 °C but increased to 100% at 320 °C. This result is in agreement with reports by Satterfield and Cocchetto [14] and Chu et al. [15]. The overall HDN reaction over the catalyst $Co_4Mo_6C_x$ is an essentially irreversible reaction controlled by kinetics rather than by thermodynamics, in agreement with earlier results [16], although the hydrogenolysis of hydrocarbons is more favoured at higher temperatures [17–19].

The product selectivity studies for pyridine HDN at different reaction temperatures show that at 160 °C pyridine conversion is very low and the main products are methane and C_5 with the selectivities of 60 and 40%, respectively. The yields for other hydrocarbons were almost negligible, suggesting that the main reaction routes at 160 °C is hydro-

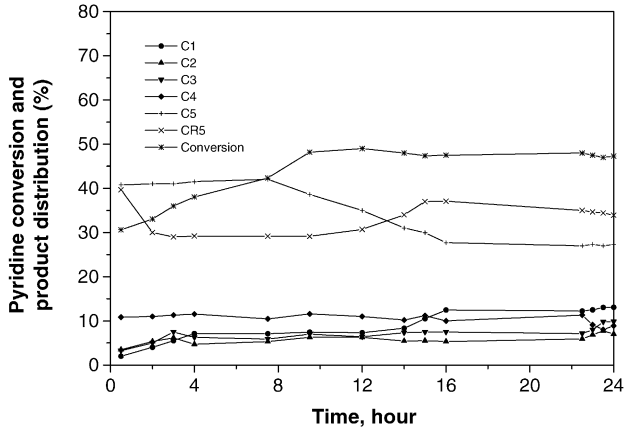

Fig. 5. Changes of products distribution in pyridine HDN over $Co_4Mo_6S_x$ catalyst, T: 380 °C, H_2/pyridine ratio: 154, P:1 bar, H_2 flow: 20 ml/min.

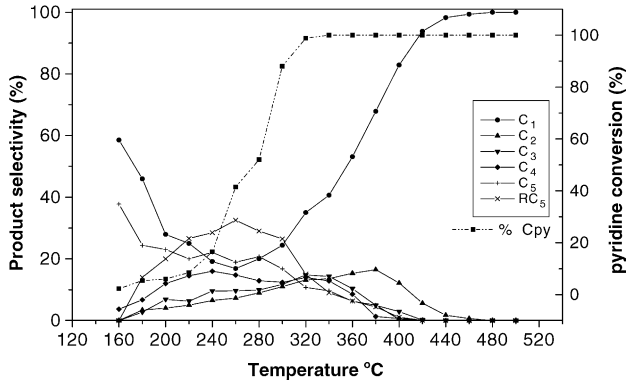

Fig. 6. Pyridine conversion and product distribution over $Co_4Mo_6C_x$ catalyst at different reaction temperature, H_2/pyridine ratio: 154, P:1 bar, H_2 flow: 20 ml/min.

genation together with some hydrogenolysis. Increasing the reaction temperature results in a dramatic decrease in the methane selectivity by ∼20%, and cyclopentane selectivity rises to ∼35% at 260 °C. Further increase of temperature causes a decrease in cyclopentane selectivity and significantly increases methane selectivity. Generally, the selectivities to C_2–C_4 are only slightly affected by changes in the reaction temperature.

The data in Fig. 6 also shows that there is more than one reaction pathway for the HDN of pyridine reaction. In the temperature range of 160–220 °C, the main products are pentane and methane and there is only very small amount of cyclopentane. The pyridine conversion was low (<10%) but stable. The higher yield of pentane without the production of cyclopentane at 160 °C is probably due to pyridine adsorption on the catalyst metal sites via the nitrogen lone-pair electrons (the so-called "end-on" bonding mode). The end-on mode would give a high yield of pentane via C–N bond cleavage. It has been proposed that pyridine hydrogenation occurs through a side-on mode of pyridine adsorption [20]. The increase of temperature above 160 °C leads to a decrease in pentane yield and a marked increase in cyclopentane yield. The change in the product distribution suggests that at the higher temperature the pyridine is attached to the metal site in a different manner from the end-on mode and this could give rise to a different reaction pathway, one that favors the production of cyclopentane. It is thought that the alternative mode is via a side-on bond using the π-electrons of the aromatic pyridine ring [7,21,22]. The side-on mode adsorption is thought to be dominant in the temperature range of 220–300 °C, leading to a dramatic increase in the conversion of pyridine. Ledoux et al. [23] has also proposed two forms of adsorption for the heterocyclic nitrogen compounds, one vertical through the protonation of the nitrogen atom on a Brønsted acid site (end-on mode) and the other mode through the π bond of the aromatic ring on a reduced site (side-on mode). Our results suggested that, at lower reaction temperatures, the ring hydrogenation (side-on mode) is slow and the C–N bond scission (end-on mode) is faster leading to the conversion of a small amount of hydrogenated pyridine to pentane and methane. At higher reaction temperatures, the pyridine conversion is high due to a fast ring hydrogenation rate (side-on mode), and the rate-determining step being the C–N bond scission.

3.3. Characterization of catalysts

The elemental chemical compositions and surface areas of the bimetllic oxide, carbide, sulfide, and nitride materials are given in Tables 1 and 2. All the CoMo carbide, nitride and sulfide catalysts show a higher surface area than the precursor $Co_4Mo_6O_x$.

The Fig. 7 shows the X-ray diffraction (XRD) patterns of the catalyst samples prepared from the same oxide precursor. After the HDN activity test, the XRD patterns of these catalysts in Fig. 8 show that most of the peaks due to residual oxide have disappeared or are significantly reduced, especially for the oxide, nitride and sulfide catalysts. It appears that that the carbide catalyst is more stable.

It is possible the H_2 and pyridine interact with Co_4Mo_4 materials to form new phases on the catalyst surface even at low reaction temperature [23]. As shown in Fig. 8, the intensity of X-ray diffraction peaks of the oxide, sulfide and nitride after reaction is severely reduced, and there is some carbon and trace of nitrogen present in all used

Table 1
Elemental compositions and surface areas of bimetallic CoMo oxide, sulfide, nitride and carbide catalysts before pyridine HDN reaction

Catalyst	Surface area $m^2\ g^{-1}$	Mo wt.%	Co wt.%	S wt.%	C wt.%	N wt.%
$Co_4Mo_6O_x$	1.96	44.8	23.8	–	–	–
$Co_4Mo_6S_x$	24.23	44.55	24.87	8.05	–	–
$Co_4Mo_6C_x$	26.80	44.63	26.14	–	6.15	–
$Co_4Mo_6N_x$	32.60	40.91	24.44	–	–	7.83

Table 2
Elemental compositions and surface areas of bimetallic CoMo oxide, sulfide, nitride and carbide catalysts after pyridine HDN reaction

Catalyst	Surface area $m^2\ g^{-1}$	Mo wt.%	Co wt.%	S wt.%	C wt.%	N wt.%
Co_4Mo_6Ox	75.92	46.69	24.56	–	3.33	1.30
Co_4Mo_6Sx	87.96	47.76	24.27	6.59	2.20	1.14
Co_4Mo_6Cx	62.97	46.62	25.65	–	4.19	0.73
Co_4Mo_6Nx	45.13	47.43	24.28	–	3.10	4.78

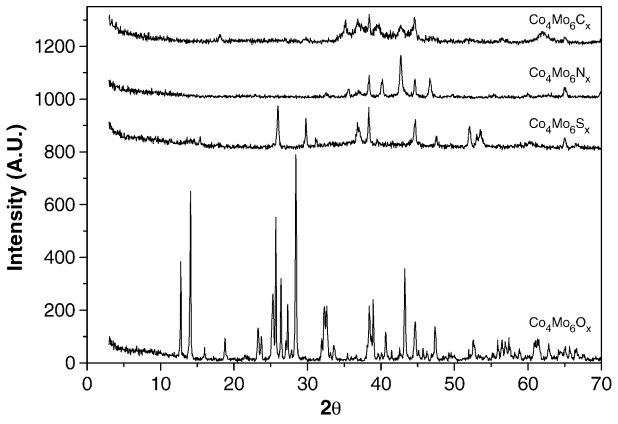

Fig. 7. XRD patterns of the bimetallic CoMo oxide, sulfide, nitride and carbide catalysts before HDN reaction.

catalysts. The surface areas of all the used catalysts were increased.

The ^{13}C NMR spectra of the used catalysts are shown in Fig. 9. All samples show a main peak at 113 ppm; this band is due to the carbon in molybdenum carbide with a fcc structure or in eta-molybdenum carbide $MoC_{(1-x)}$ [11,12]. We note that the main band of ^{13}C NMR in the molybdenum carbide occurs at 275 ppm. The ^{13}C NMR peak at 275 ppm is very weak and noisy, implying that almost no hcp-molybdenum carbide is formed in the bimetallic oxide, nitride and sulfide catalysts, which is in agreement with the XRD results. A small ^{13}C NMR peak at 208 ppm is seen in the spent $CoMoC_x$, $CoMoN_x$, and $CoMoS_x$.

3.4. Activation energy of different catalysts

The apparent activation energies (Eap) of each catalyst were calculated from Arrhenius plots, and the results are given in Table 3.

The apparent activation energies for HDN are 19–30 kJ/mol and are similar to those for $NiMoS_x$ catalysts [24]. It is clear that the least active catalyst $CoMoS_x$ has the highest apparent activation energy, 29.8 kJ/mol. The $CoMoN_x$ has an apparent activation energy of 25.6 kJ/mol, lower than the sulfide catalysts, and equivalent to the un-promoted Mo_2N catalyst, whose activation energy is 7.16 kcal/mol [25]. This suggests that the activation site of the $CoMoN_x$ is similar to that of the Mo_2N catalyst. The apparent activation energy of the carbide catalyst is 21.5 kJ/mol, which is lower than the sulfide and nitride catalysts, while its activity is also higher than those two catalysts. The apparent activation energy of the catalyst derived from $CoMoO_x$ may be in fact arise from cobalt metal energy for a cobalt metal formed in the initial hydrogen pre-treatment step.

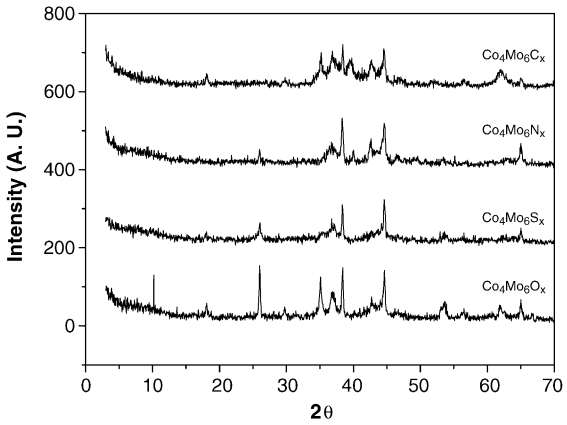

Fig. 8. XRD patterns of the bimetallic CoMo oxide, sulfide, nitride and carbide catalysts after HDN reaction.

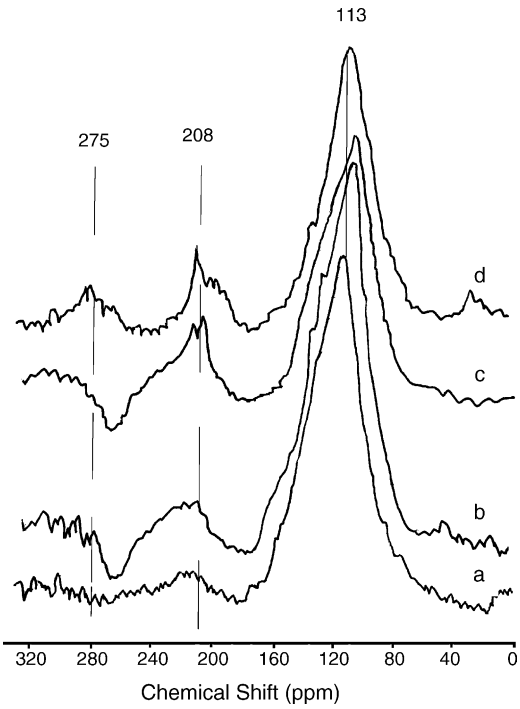

Fig. 9. ^{13}C NMR of CoMo bimetallic catalysts after HDN reaction, (a) $CoMoO_x$, (b) $CoMoS_x$, (c) $CoMoN_x$, and (d) $CoMoC_x$.

Table 3
Apparent activation energy of CoMo bimetallic oxide, sulfide, nitride and carbide catalysts for pyridine HDN reaction

Catalyst	Oxide (kJ/mo)	Sulfide (kJ/mo)	Carbide (kJ/mo)	Nitride (kJ/mo)
Activation energy of the fresh catalyst	23.5	29.8	21.5	25.6
Activation energy of the spent catalyst	28.2	27.3	19.1	28.5

4. Conclusion

The Co_4Mo_6 carbide catalyst shows the highest activity for pyridine HDN. It is believed that the carbide phase is more structure stable than other phases.

The preliminary HDN activity of the catalysts is in order of $CoMoC_x \sim CoMoN_x \sim CoMoO_x > CoMoS_x$. The stability order of the first three catalysts is $CoMoC_x > CoMoN_x > CoMoO_x$, and their activities decrease with the time on stream. The reaction temperature has a significant effect on HDN products and hence the mechanism over $Co_4Mo_6C_x$. Two types of pyridine adsorption on the carbide catalyst surface may occur in the HDN reaction. Higher initial activity of the bimetallic oxide may be due to the presence of metallic cobalt particles formed in the pre-treatment. The oxide and nitride materials were converted into carbide during the HDN reaction.

References

[1] J.G. Speight, Petroleum Chemistry and Refining, Taylor and Francis, 1998.
[2] J.C. Schlatter, S.T. Oyama, J.E.III Metcalfe, J.M. Lambert Jr., Ind. Eng. Chem. Res. 27 (1988) 1648.
[3] K.S. Lee, H. Abe, I.A. Reimer, A.T. Bell, J. Catal. 139 (1993) 34.
[4] H. Abe, T. Cheung, A.T. Bell, Catal. Lett. 21 (1993) 11.
[5] C.W. Colling, L.T. Thompson, J. Catal. 146 (1994) 193.
[6] S. Ramanathan, S.T. Oyama, J. Phys. Chem. 99 (1995) 16365.
[7] J.G. Choi, J.R. Brenner, L.T. Thompson, J. Catal. 154 (1995) 33.
[8] S. Li, J.S. Lee, T. Hyeon, K. Suslick, Appl. Catal. A: Gen. 184 (1999) 1.
[9] C.C. Yu, S. Ramanathan, B. Dhandapani, J.G. Chen, S.T. Oyama, J. Phys. Chem., B 101 (1997) 512.
[10] V. Schwartz, S.T. Oyama, J.G. Chen, J. Phys. Chem., B 104 (2000) 8800.
[11] T-C. Xiao, A.P.E. York, H. Al-Megren, J.B. Claridge, V.C. Williams, H-T. Wang, M.L.H. Green, J. Catal. 202 (2001) 100.
[12] T-C. Xiao, A.P.E. York, V.C. Williams, H. Al-Megren, A. Hanif, X-Y. Zhou, M.L.H. Green, Chem. Mater. 12 (2000) 3896.
[13] T-C. Xiao, A.P.E. York, H. Al-Megren, J.B. Claridge, H-T. Wang, M.L.H. Green, Chimie des surfaces et catalyse, C.R. Acad. Sci. (Paris) Ser. IIc Chim. /Chem. 3 (2000) 451.
[14] C.N. Satterfield, J.F. Cocchetto, AIChE. J. 21 (1975) 1107.
[15] Y. Chu, Z. Eei, S. Yang, C. Li, Q. Xin, E. Min, Appl. Catal. A: Gen. 176 (1999) 17.
[16] T. Kabe, A. Ishihara, W. Qian, Hydrodesulfurization and Hydrodenitrogenation Chemistry and Engineering, Wiley-VCH, 1999.
[17] J.F. Cocchetto, C.N. Satterfield, Ind. Eng. Chem. Process Des. Dev. 15 (1976) 272.
[18] J.F. Cocchetto, C.N. Satterfield, Ind. Eng. Chem. Process Des. Dev. 20 (1981) 49.
[19] A. Bunch, L. Zhang, G. Karakas, U.S. Ozkan, Appl. Catal. A: Gen. 190 (2000) 51.
[20] C. Moreau, P. Geneste, in: J.B. Moffat (Ed.), Theoretical Aspects of Heterogeneous Catalysis, Van Nostrand Reinhold Catalysis Series, 256, 1990.
[21] K. N. Mathur, Z. Sarbak, N. Islam, H. Kwart, J. R. Katzer, Tenth and Eleventh Quarterly Reports for the Period August 16, 1981 to February 15, 1982; Prepared for Office of Fossil Energy, Department of Energy, Washington, DC, 1982.
[22] K. N. Mathur, M. D. Schrenk, H. Kwart, J. R. Katzer, Final report for the Period September 15, 1978 to September 1981; Prepared for Office of Fossil Energy, Department of Energy, Washington, DC, 1982.
[23] M.J. Ledoux, P.E. Puges, G. Maire, J. Catal. 76 (1982) 285.
[24] C.D. Ajaka, R.S. Mann, Indian J. Technol. 31 (1993) 131.
[25] C.D. Ajaka, R.S. Mann, K.C. Khulbe, Indian J. Chem. Technol. 1 (2) (1994) 75.